Separated Fringe Packet Observations with the CHARA Array. III. The Very High-eccentricity Binary HR 7345

C. D. Farrington[1] , Francis C. Fekel[2] , G. H. Schaefer[1] , and T. A. ten Brummelaar[1]
[1] The CHARA Array, Mt. Wilson Observatory, Mt. Wilson, CA 91023, USA; farrington@chara-array.org
[2] Tennessee State University, 3500 John A. Merritt Boulevard, Box 9501, Nashville, TN 37209, USA
Received 2018 May 7; revised 2018 August 2; accepted 2018 August 2; published 2018 September 10

Abstract

After an 11-year observing campaign, we present the combined visual–spectroscopic orbit of the formerly unremarkable bright star HR 7345 (HD 181655, HIP 94981, GJ 754.2). Using the Separated Fringe Packet method with the CHARA Array, we were able to determine a difficult-to-complete orbital period of 331.609 ± 0.004 days. The 11-month period causes the system to be hidden from interferometric view behind the Sun for three years at a time. Due to the high-eccentricity orbit of about 90% of a year, after 2018 January the periastron phase will not be observable again until late 2021. Hindered by its extremely high eccentricity of 0.9322 ± 0.0001, the double-lined spectroscopic phase of HR 7345 is observable for 15 days. Such a high eccentricity for HR 7345 places it among the most eccentric systems in catalogs of both visual and spectroscopic orbits. For this system, we determine nearly identical component masses of $0.941 \pm 0.076\,M_\odot$ and $0.926 \pm 0.075\,M_\odot$ as well as an orbital parallax of 41.08 ± 0.77 mas.

Key words: binaries: close – infrared: stars – stars: individual (HD 181655) – techniques: high angular resolution – techniques: interferometric – techniques: spectroscopic

Supporting material: machine-readable tables

1. Introduction

1.1. Observational History of HR 7345

HR 7345 (HD 181655, HIP 94981, GJ 754.2) is a 6th magnitude star in the constellation Lyra near the boundary line with Cygnus and seemed for decades to be an unremarkable system aside from its proximity to the Sun. We discovered it to be a highly eccentric binary, even though it had not been identified in previous multiplicity surveys. It was included as part of a David Dunlap Observatory (DDO) radial velocity survey of 681 relatively bright stars for which velocities were lacking (Young 1945). A decade later, Halliday (1955) used the same DDO spectra to calculate the luminosity and spectroscopic parallax ($\pi_{\rm sp} = 79.7$ mas) for the system and classified its spectrum as G8 V. Two years later, Crissman (1957) determined its trigonometric parallax ($\pi_{\rm trig} = 39$ mas) from photographic plates and found a value very close to the modern Hipparcos (Gaia Collaboration et al. 2016) measurement ($\pi_{\rm Hip} = 39.34$ mas). During the next 20 years, it was spectroscopically and photometrically measured and classified, with no hint of variability, even being listed as a radial velocity standard star by Beavers et al. (1979) from 20 measurements over three years at the Fick Observatory. The system was measured six more times between 1978 and 1983 at the McDonald Observatory 2.1 m telescope where it just barely fell outside of the 2.5σ error limit for their definition of a "radial-velocity standard star" (Barnes et al. 1986). HR 7345 was even observed in the early eighties by the primary author's thesis advisor with speckle interferometry (McAlister et al. 1987) on the Kitt Peak 4 m telescope, which gave a null result for their single observation in 1985. The timing of that measurement was particularly unlucky, as the companion would have been just coming out of periastron but not yet separated enough for easy resolution on the 4 m telescope. Radial-velocity data were again acquired during the CORAVEL survey

of Duquennoy et al. (1991), who searched for companions of solar-type stars in the solar neighborhood. Twelve measurements of HR 7345, taken over the course of 1200 days between 1983 and 1989, indicated very little velocity variation. In retrospect, their timing was most unfortunate, as they were tantalizingly close to the very short observing window when the system would have exhibited double lines between 1983 and 1985. Unfortunately, again because of the very limited window, nearly all subsequent observations of HR 7345 failed to show evidence of binarity (Duflot et al. 1995; Fehrenbach et al. 1997; Nidever et al. 2002; Gray et al. 2003; Halbwachs et al. 2003; Nordström et al. 2004; Valenti & Fischer 2005; Holmberg et al. 2009; Crifo et al. 2010; Soubiran et al. 2013; Gaia Collaboration et al. 2016). In fact, out of all the radial velocity observations collected during the past 50 years, only one, an ELODIE spectrum acquired in 2000 November, was close enough to periastron to exhibit partial separation of its double lines (Prugniel et al. 2007). Finally, the Palomar-Testbed Interferometer observed the system over 40 times between 1998 and 2005 and saw no evidence of a companion with their 86–110 m baselines and deemed it to be a suitable calibrator star (van Belle et al. 2008). Further inquiry into the reasons why it was not detected are ongoing, but due to orbital elements projected backwards, there were several years when the companion should have been detectable.

1.2. High-eccentricity Binaries

As is often the case, many of the most interesting systems are discovered by accident. Although not originally considered until many observations were obtained, the importance of surveying high-eccentricity binary systems cannot be overstated. Characterizing high-eccentricity systems can provide insight into the statistics of stellar formation mechanisms, multiplicity fractions, and star formation rates, which all lead to the Inital Mass Function (Ambartsumian 1937; Bate 2009;

Tokovinin & Kiyaeva 2016). It is well known that both visual and spectroscopic observations can easily miss a significant fraction of high-eccentricity systems (Duquennoy & Mayor 1991; Raghavan et al. 2010; Griffin 2012) by something as simple as timing where either the relative motion of the components in the visual case is very slow for most of their orbital period, or the relatively short time when the spectra would exhibit double lines. This combined with the wide variation of inclinations and distances means even discovering high-eccentricity systems is often left up to a chance observation. Once found, these systems can help define the limits of the eccentricity distributions (Raghavan et al. 2010), relations between period and eccentricity (Finsen 1936), and the mechanism that creates such extreme systems (See Section 5).

2. Observations

During the primary author's dissertation research, one of the first systems observed was HR 7345 in a search for companions that were missed in the multiplicity survey of Duquennoy & Mayor (1991). It was suspected that, prior to the Hipparcos mission, there could well be systems in the aforementioned multiplicity survey that were not within the 22 pc distance parameter as well as the possibility of undiscovered companions that were below the resolution capability of single aperture interferometry. In this case, HR 7345 was both the first system in that survey to exhibit multiple fringe packets and the first previously unknown companion discovery. Unbeknown to us, its very high eccentricity and nearly one-year orbital period closely aligned periastron with its conjunction with the Sun from 2005 to 2010. Thus, after five years of observations, all the measurements were loosely clustered in the N–S direction with very little movement in position angle or separation. The following year, we were able to catch a fast moving phase in the E–W direction that returned our interest to the system, and HR 7345 was added to a list of systems to be monitored more often. As its components are of nearly equal brightness in the infrared, the fringe packet amplitudes are nearly identical, and so, it was not until the end of 2015 that we identified the correct period with the help of spectroscopic observations. By the time we were able to pinpoint the time of periastron passage, we were unable to acquire interferometric observations during that fast moving phase due to unfavorable weather conditions at Mount Wilson during 2016 March and 2017 February. Fortunately, during predicted periastron passage on 2018 January 24, we were able to use the three longest baselines of the CHARA Array in the last hour of the night when the star was just 16° above the horizon to get three observations to pin down the unobserved part of the orbit.

2.1. Interferometric Observations

We obtained observations of HR 7345 from 2005 October through 2018 January with multiple combinations of baselines using the Classic and CLIMB (ten Brummelaar et al. 2013) beam combiners of the CHARA Array at Mount Wilson Observatory in southern California (ten Brummelaar et al. 2005). During the first three years, the Separated Fringe Packet (SFP) project (Farrington et al. 2010, 2014, hereafter referred to as Paper I and Paper II, respectively) only had access to the Classic beam combiner, which could only observe with one baseline at a time and took significant time to reconfigure. As such, there were sometimes gaps of one to several days between different baseline measurements. Luckily, during this period the observation windows lined up with the very slow moving apastron phase. With the advent of CLIMB in 2009, we were able to collect data on three baselines within 15 minutes of acquisition. Data were routinely taken with the CHARA Array's outer telescope triangle (S1-W1-E1), as they have the greatest separation and are able to probe the smallest separations. The setup of the Array in general, the SFP method, error sources, and the acquisition/reduction of data are discussed in detail in Paper I. The conversion of reduced data into "on-sky 2D" measurements is expanded upon and described in Paper II. For the final astrometric measurement, the predicted separation was far below the resolution limit of the SFP process, so three calibrated brackets were taken using the traditional visibility method with the same triangle mentioned previously and using HD 174602 and HD 173649 as calibrators with a C1-O-C2-C1-O-.. sequence and calibrator diameters of 0.356 and 0.388 mas, respectively (Bourges et al. 2014). Data were reduced using a pipeline developed by J. D. Monnier, using the general method described in Monnier et al. (2011) and extended to three beams (e.g., Kluska et al. 2018). The calibrated OIFITS file is available through the Optical Interferometry DataBase (OIDB)[3] or upon request.

All one-dimensional (1D) observations from the CHARA Array and subsequent two-dimensional (2D) calculations from 2005 to 2018 are listed in Table 1. The first four columns characterize the 1D measurements taken by a single baseline (time, baseline length, fringe separation, and position angle of the baseline), while the last six columns are the average position of the detected companion with associated errors. The conversion of time frames in the averages is to consolidate to one reference frame congruent with the spectroscopic observations described in the following section. The final line of Table 1 contains the periastron observation taken during 2018 January. We solved for the binary position on UT 2018 January 24 using the adaptive grid search procedure described in Schaefer et al. (2016). We derived a flux ratio of 1.07 ± 0.02 in the K-band at the position listed in the last line of Table 1.

2.2. Spectroscopic Observations

We obtained observations of HR 7345 from 2014 June through 2018 January with the Tennessee State University (TSU) 2 m automatic spectroscopic telescope (AST) and a fiber-fed echelle spectrograph (Eaton & Williamson 2007). That telescope is situated at Fairborn Observatory near Washington Camp in southeastern Arizona. The detector is a Fairchild 486 CCD having a 4096 × 4096 array of 15 μm pixels. For our observations, we used a 200 μm fiber that results in a spectral resolution of 0.24 Å. The signal-to-noise ratio of the spectra was typically about 90 per resolution element at 6000 Å.[4]

Fekel et al. (2009) provided an extensive general description of velocity measurement of the Fairborn AST spectra. In the case of HR 7345, we used a solar line list that covered the wavelength range 4920–7100 Å and fitted the individual lines with a rotational broadening function (Fekel & Griffin 2011;

---

[3] OIDB searchable database located at http://oidb.jmmc.fr/index.html.
[4] The echelle spectra FITS format files are available at http://ast2.tsuniv.edu/HD_181655/.

Table 1
Visual Binary Measurements for SFP System HR 7345

MJD(1D)	B(m)	ρ(mas)	θ(degree)	HJD(2D)	JY_{calc}	ρ(mas)	ρ_{err}(mas)	θ	θ_{err}
53890.267	270.1	73.57	4.98						
53891.208	275.73	73.15	132.82						
53892.251	279.31	30.5	230.15						
53892.28	297.19	37.11	226.82						
53892.384	328.03	65.04	210.66	2453892.59802	2006.42538	63.13	0.9	341.1	0.82
53987.253	330.01	34.97	2.58						
53988.221	330.29	41.28	9.42						
53989.2249	271.08	64.26	308.46						
53989.3145	227.63	47.34	294.65						
53990.242	265.28	76.99	305.13						
53991.1785	330.65	85.27	17.32						
53991.2655	330.02	68.84	357.1	2453989.74113[a]	2006.69609	87.76	7.05	352.08	4.58
54249.4004	276.69	61.62	24.1						
54249.4071	277.11	61.02	22.84						
54254.3993	177.45	80	346.58						
54254.4941	174.47	78.8	327.75	2454251.92110	2007.41252	79.62	3.74	344.81	2.69
54323.2745	248.13	87.12	11.82						
54324.3997	248.03	91.14	343.41						
54329.1695	275.11	88.37	335.67						
54330.4124	330.63	89.98	339.91	2454327.00411	2007.61756	92.88	1.53	351.32	0.93
54393.1171	271.57	53.78	308.82						
54393.1858	242.88	42	297.83						
54393.231	330.66	79.77	341.94						
54393.2411	330.62	78.29	339.77	2454393.69400	2007.79930	78.62	4.71	359.5	3.43
54697.2614	248.12	84.4	9.66						
54697.3486	248.12	85.59	350.19						
54699.3158	248.06	85.69	356.1						
54699.3208	248.07	86.4	354.9						
54699.3942	247.63	82.28	339.01						
54704.1787	247.29	76.88	337						
54704.2825	248.38	86.94	359.39	2454701.77290	2008.63972	87.25	0.73	355.42	0.48
55115.1294	307.13	32.67	61.9						
55115.1631	265.04	23.91	305.02						
55115.1839	330.00	52.28	358.3	2455115.65951	2009.77592	53.6	0.63	8.99	0.67
55346.3611	272.87	82.92	342.19						
55346.4009	327.78	74.37	31.08						
55346.4467	313.37	18.52	73.45	2455347.38584	2010.40904	87.16	2.73	356.75	1.79
55439.17945	278.24	44.14	324.48						
55439.1809	312.46	22.23	75.75						
55439.1845	330.32	56.58	23.76						
55439.2244	330.6	57.97	15.07						
55439.2288	276.15	35.1	313.42	2455439.70121	2010.66310	59.17	0.86	7.13	0.84
55445.1374	246.68	53.66	25.48						
55445.1407	154.22	19.31	70.45						
55445.1439	177.44	50.82	345.69	2455445.64292	2010.67937	55.2	3.57	2.86	3.70
55468.1399	248.13	36.01	11.96						
55468.1434	154.95	28.83	56.14						
55465.147	177.18	26.15	338.59	2455468.64471[a]	2010.74234	35.82	7.82	20.68	12.39
55516.1213	237.00	32.69	296.5						
55516.1258	266.79	14.7	213.59						
55516.1316	330.46	38.46	167.71	2455516.62513	2010.87372	40.59	0.25	330.4	0.34
55750.3251	278.27	55.3	324.29						
55750.3276	312.38	21.45	75.88						
55750.3312	330.26	66.13	24.07	2455750.83091	2011.51494	70.95	0.32	3.32	0.76
55775.2151	275.49	47.36	334.38						
55775.2183	210.96	54.44	352.11						

Table 1
(Continued)

MJD(1D)	B(m)	ρ(mas)	θ(degree)	HJD(2D)	JY_{calc}	ρ(mas)	ρ_{err}(mas)	θ	θ_{err}
55775.2293	304.58	14.4	82.47						
55775.2325	328.3	52.0	30.17	2455775.72680	2011.58309	56.42	0.04	7.28	0.04
55781.1517	177.33	51.55	1.96						
55781.159	239.99	45.58	35.64						
55781.3067	175.1	38.37	329.13						
55781.3119	152.12	39.23	49.8						
55781.3149	248.07	50.56	4.73	2455781.74181	2011.59958	51.1	0.9	9.83	0.99
55782.3172	270.81	23.86	308.27						
55782.3209	301.25	35.83	57.27						
55782.3248	330.13	51.01	6.04	2455782.82393[a]	2011.60251	51.49	4.38	10.97	4.96
55796.15	274.78	29.46	336.45						
55796.1535	296.71	14.21	86.26						
55796.157	326.09	36.43	33.43						
55796.1897	277.83	25.73	326.62						
55796.193	310.74	17.28	77.96						
55796.1961	329.88	36.73	25.94	2455796.67591	2011.64044	38.14	1.37	15.91	2.08
55808.1349	246.71	15.2	328.22						
55808.1388	243.29	9.31	86.92						
55808.1421	246.61	25.03	25.72						
55808.2781	231.83	20.17	54.32						
55808.2811	248.07	22.37	355.81	2455808.6765[a]	2011.67336	19.7	11.06	24.68	4.77
55817.1117	276.43	$\lesssim$5.00	331.59						
55817.1169	244.09	15.58	86.37						
55817.1212	277.43	13.29	21.75	2455817.61864[a]	2011.69778	17.2	7.63	61.45	22.89
55829.2295	256.35	18.48	301.6						
55829.2337	283.33	2.92	45.38						
55829.2378	330.05	11.98	356.26						
55829.2602	239.47	17.07	297.04						
55829.2669	267.39	5.94	34.07						
55829.2709	330.41	13.62	348.44	2455829.74792	2011.73100	17.5	2.84	319.45	9.30
55843.1036	277.97	34.88	317.28						
55843.1119	330.64	24.24	16.63						
55843.1961	253.91	29.55	300.81						
55843.2022	280.49	11.42	43.5						
55843.2076	330.11	30.77	354.35	2455843.66510	2011.76910	34.68	1.48	331.39	2.44
56052.5008	278.33	65.96	143.79						
56053.4454	244.54	70.32	210.35						
56053.4514	150.23	21.55	255.33						
56053.4546	177.4	80.97	170.95						
56053.473	246.75	72.82	205.25						
56053.4812	154.5	28.4	249.94	2456053.80120	2012.34442	81.5	0.99	359.19	0.71
56076.4242	177.43	67.75	163.86						
56076.4289	155.64	37.11	247.25						
56076.4307	247.64	68.06	159.02						
56076.485	154.27	44.87	234.35						
56076.4897	175.7	61.12	150.74						
56076.4941	248.1	69.31	187.69	2456076.96660	2012.40785	71.25	1.54	2.73	1.24
56077.392	275.79	62.94	153.5						
56077.3944	302.16	13.24	263.76						
56077.3992	327.66	62.83	211.28						
56077.4767	248.13	71.33	191.19						
56077.4793	154.48	45.64	234.88						
56077.4846	175.83	62.52	151.16	2456077.93962	2012.41051	72.49	1.56	3.45	1.24
56116.24469	177.32	49.3	179.69						
56116.24826	202.91	18.56	259.21						
56116.25173	291.68	41.7	221.66						
56116.42285	236.22	16.74	120.8						

Table 1
(Continued)

MJD(1D)	B(m)	ρ(mas)	θ(degree)	HJD(2D)	JY_{calc}	ρ(mas)	ρ_{err}(mas)	θ	θ_{err}
56116.42728	234.39	36.53	236.21						
56116.43033	248.05	47.59	177.37	2456116.84052	2012.51700	49.66	1.45	11.36	1.66
56131.18872	271.16	31.06	168.52						
56131.19272	271.42	29.56	167.41						
56131.19652	270.98	15.41	275.00						
56131.20019	317.43	31.47	219.96						
56131.23108	274.64	26.79	156.85						
56131.23569	296.49	14.85	266.35						
56131.23937	326.12	33.89	213.39						
56132.15739	238.62	29.95	173.84						
56132.16195	192.73	$\lesssim$5.00	288.72						
56132.16563	232.54	31.61	220.4						
56132.35159	174.54	32.58	147.89						
56132.35758	151.00	32.26	227.72						
56132.36157	248.06	31.82	183.19	2456132.18418	2012.55901	34.76	2.15	20.67	3.55
56141.20961	297.08	12.77	266.4						
56141.21415	297.9	23.3	216.56						
56141.35505	236.15	$\lesssim$5.00	120.76						
56141.3618	291.29	20.82	230.56						
56141.36727	300.95	21.98	183.13	2456141.80458	2012.58535	23.54	0.9	27.65	2.17
56148.19281	275.35	$\lesssim$5.00	154.79						
56148.2227	309.19	12.67	259.37						
56148.22548	329.55	12.03	207.15	2456148.72519	2012.60428	13.9	1.46	47.66	6.04
56162.25105	248.12	13.27	9.45						
56162.25653	153.64	$\lesssim$5.00	52.9						
56162.2631	175.13	22.99	329.2						
56162.27947	248.06	15.21	3.05						
56162.28356	149.85	$\lesssim$5.00	45.68						
56162.28723	172.91	24.9	325.11	2456162.77546	2012.64276	23.1	2.5	319.35	6.22
56186.24046	261.4	38.24	303.44						
56186.24455	289.15	13.98	49.16						
56186.24988	330.00	40.7	358.69						
56186.28818	235.69	37.15	296.23						
56186.29246	266.21	24.64	33.13						
56186.2966	330.45	46.66	347.72	2456186.77049	2012.70847	46.31	2.17	335.53	2.69
56195.1479	277.37	47.62	315.61						
56195.15299	311.45	$\lesssim$5.00	246.52						
56195.15704	330.57	43.47	14.62						
56195.24809	245.41	40.82	298.45						
56195.25151	273.78	22.71	38.36						
56195.25502	320.24	49.71	351.64	2456195.70359	2012.73293	51.89	2.35	337.47	2.59
56245.07452	263.2	55.46	304.19						
56245.08012	290.44	32.53	50						
56245.08698	330.00	84.27	359.11	2456245.57954	2012.86949	81.08	7.34	346.98	5.19
56414.46069	210.95	70.75	353.93						
56414.4654	214.64	30.2	72.75						
56414.47028	326.88	57.76	32.43						
56414.49626	210.94	73.2	346.07						
56414.50139	220.89	36.77	65.72						
56414.50395	329.91	56.75	25.84	2456414.98359	2013.33329	70.1	9.27	4.13	7.57
56438.36719	272.58	48.7	343.13						
56438.37547	321.58	47.3	37.47						
56438.41196	177.43	53.21	348.45						
56438.41639	153.49	29.56	71.58						
56438.42247	246.92	54.51	24.64	2456438.90039	2013.39877	55.76	2.99	11.31	3.07
56445.39279	177.43	46.9	348.5						
56445.40031	246.79	49.29	25.11						
56445.42323	278.3	32.64	324.1						

Table 1
(Continued)

MJD(1D)	B(m)	ρ(mas)	θ(degree)	HJD(2D)	JY_{calc}	ρ(mas)	ρ_{err}(mas)	θ	θ_{err}
56445.42937	312.85	23.86	74.99						
56445.43394	330.41	48.72	23.04	2456445.91792	2013.41798	50.35	1.14	12.96	1.83
56461.31538	273.61	30.52	339.9						
56461.32094	290.43	9.38	88.7						
56461.32531	324.35	34.8	35.24	2456461.82305	2013.46152	37.07	0.46	13.78	0.71
56518.21606	278.04	32.28	198.81						
56518.21948	249.3	13.36	181.51						
56518.22234	278.28	46.42	144.22						
56518.28757	278.76	40.09	183.73						
56518.29165	245.37	$\lesssim$5.00	245.26						
56518.29646	272.05	42.04	129.18	2456518.75849	2013.61740	46.33	1.01	334.42	1.26
56566.1015	156.22	19.83	244.27						
56566.10548	210.68	72.2	160.99						
56566.10922	278.55	63.22	194.06						
56566.24919	235.06	49.7	116.1						
56566.25368	210.1	45.29	142.36						
56566.25728	278.2	73.17	162.28	2456566.68059	2013.74861	73.3	4.04	346.7	3.17
56772.48997	245.74	53.27	208.03						
56772.49743	177.43	50.56	168.39						
56772.50785	246.9	51.62	204.72						
56772.50972	154.64	26.19	249.68						
56772.51533	177.44	49.05	164.53						
56772.52139	155.6	30.73	247.37	2456773.00713	2014.31351	54.51	1.89	10.14	1.98
56826.36376	248.13	19.83	324.12						
56827.3513	247.3	20.15	326.82						
56827.35608	307.03	12.33	260.96						
56827.44708	244.36	22.25	306.09						
56827.46087	301.39	10.52	10.15	2456827.69816	2014.46323	20.91	1.43	311.81	3.95
56935.14887	273.59	67.45	310.48						
56935.15368	304.99	26.97	60.1						
56935.15879	330.24	71.62	8.41	2456935.65478	2014.75881	80.56	5.34	347.28	3.78
57566.26909	271.84	79.94	345.73						
57566.27375	275.62	27.12	273.61						
57566.27962	319.97	48.68	38.53	2457566.77685	2016.48672	80.83	1.53	344.65	1.09
57573.31056	210.97	82.41	348.99						
57573.31825	219.78	18.99	67.69						
57573.32459	329.46	60.21	27.42	2457573.82070	2016.50600	80.21	4.33	350.87	3.09
57650.21089	173.26	79.92	325.63						
57650.21478	149.01	60.47	44.23						
57650.21898	248.05	88.95	0.17						
57650.27145	162.76	72.15	316.64						
57650.27702	138.5	77.35	24.46						
57650.28224	248.11	77.84	346.27	2457650.74032	2016.71661	90.61	2.08	354.54	1.32
				2458143.06401	2018.06453	3.4	0.04	199.82	0.59

Notes. All CHARA Array SFP observations for HR 7345. Each set of 1D vector observations (along with the projected baseline length and epoch of observation) in columns one through four were combined to create the true location of the secondary and average time of all the data points defined in the last six columns with position angle being defined as standard north through east without correcting for precession. The MJD from the 1D measurements was converted to HJD-2400000 to match the time coordinates of the spectroscopic data included in Table 2. Additionally, we omitted the measurement from HJD 56478.4694 (sep = 25.57, PA = 131.04) because of the very large discrepancy with the orbital fit and because it was measured from three points on only one baseline and was near periastron. The final line of the table is the measurement taken by the three-baseline CLIMB during periastron in 2018 January and does not include 1D information.
[a] The residuals from these measurements compared with the orbit fit were more than three times the measurement error, so we increased their uncertainties by a factor of 10 to minimize their impact on the orbit fit.

(This table is available in machine-readable form.)

Lacy & Fekel 2011). Because the orbit of HR 7345 has an extremely high eccentricity, the lines of its two nearly identical components appear as highly blended, single features for the vast majority of its orbit, and so a single velocity was determined for most of those observations. The maximum velocity separation in that part of the orbit occurs at about phase 0.75 and is just 4 km s^{-1}. However, once the velocities of the two components began to change significantly near periastron passage, causing the single lines to broaden and weaken in strength, we determined velocities for both components by fitting the still very blended profiles with two rotational broadening functions. The starting values for the depths and widths of the components in the blends were determined from those values found for well separated lines at phases very close to periastron. Velocities from the AST CCD spectra have a zero-point offset of -0.6 km s^{-1} relative to the absolute radial velocities cataloged in Scarfe (2010). Thus, we added 0.6 km s^{-1} to our measured velocities. All of the spectroscopic observations for this system are listed in Table 2.

3. Orbital Solution

3.1. Interferometric Orbit

We determined an initial set of orbital parameters by fitting the 44 interferometric positions using the three-dimensional grid search procedure described by Schaefer et al. (2006). We then refined the orbital parameters with a Newton-Raphson method to minimize the χ^2 value between the measurements and the orbit fit by calculating a first-order Taylor expansion for the equations of orbital motion. We adopted an iterative approach to adjust the weights of each measurement. First, we uniformly scaled the uncertainties on the positions to force the reduced χ^2_ν to equal unity (where ν is the degree of freedom). If the residual from any measurement compared with the orbital fit was more than three times the measurement error, we adjusted the weight of that measurement such that the uncertainty of the data point increased by a factor of 10. We then re-computed the orbital fit, uniformly re-scaled all of the uncertainties to force the reduced χ^2_ν to equal unity, and compared the residuals to adjust the individual weights again. We repeated this process until no more uncertainties were adjusted. In the end, a total of five measurements had their uncertainties adjusted. The final scaled uncertainties adopted for all measurements are reported in columns eight and ten of Table 1.

3.2. Spectroscopic Orbit

Our very first AST spectrum showed partially separated double lines that had nearly equal depths, but without sufficient knowledge of the orbital elements, our next spectrum was not obtained until nearly two weeks later, by which time the partially blended, double-lined profile had become a narrow single-lined profile. A spectrum 342 days later showed a broadening and weakening of the single-lined profile, but that was the last spectrum obtained before monsoon season. Nearly 330 days later, there was again an indication that modest velocity changes had occurred, when one spectrum showed the component lines partially resolved. Despite the very limited number of spectra with indications of velocity changes, the very extensive number of single-lined spectra suggested a high-eccentricity orbit with a

Table 2
Spectroscopic Observations for System HR 7345

HJD—2400000	K_1(km s^{-1})	K_1 Weight	K_2(km s^{-1})	K_2 Weight
51853.2540	−4.51	1.0	8.49	1.0
56822.6593	−8.57	1.0	12.52	1.0
56835.9192	−1.74	0.0	6.19	0.0
56898.7493	2.07	0.0	⋯	⋯
56934.7889	2.11	0.0	⋯	⋯
56979.6116	2.06	0.0	⋯	⋯
57047.0342	2.21	0.0	⋯	⋯
57080.9864	2.03	0.0	⋯	⋯
57120.8380	2.11	0.0	⋯	⋯
57164.8253	−2.67	0.0	6.82	0.0
57282.6075	1.96	0.0	⋯	⋯
57283.6763	2.00	0.0	⋯	⋯
57417.0219	1.99	0.0	⋯	⋯
57432.0365	1.74	0.0	⋯	⋯
57451.9356	1.67	0.0	⋯	⋯
57474.8658	−4.63	0.5	8.21	0.5
57487.8338	−6.75	0.5	10.13	0.5
57497.8088	−2.57	0.0	5.88	0.0
57500.9954	−1.87	0.0	5.68	0.0
57509.7723	−0.51	0.0	4.48	0.0
57514.8204	1.92	0.0	⋯	⋯
57515.8037	1.94	0.0	⋯	⋯
57516.8238	1.94	0.0	⋯	⋯
57517.7608	2.10	0.0	⋯	⋯
57524.7618	2.00	0.0	⋯	⋯
57527.7524	1.89	0.0	⋯	⋯
57530.7197	1.91	0.0	⋯	⋯
57535.9460	1.86	0.0	⋯	⋯
57538.7014	1.78	0.0	⋯	⋯
57580.7087	1.75	0.0	⋯	⋯
57629.8280	2.07	0.0	⋯	⋯
57678.7602	2.06	0.0	⋯	⋯
57716.6133	1.96	0.0	⋯	⋯
57717.6021	2.14	0.0	⋯	⋯
57722.6474	2.06	0.0	⋯	⋯
57748.5772	2.00	0.0	⋯	⋯
57761.0544	1.91	0.0	⋯	⋯
57762.0435	1.88	0.0	⋯	⋯
57763.0429	1.79	0.0	⋯	⋯
57765.0411	1.92	0.0	⋯	⋯
57777.0446	1.71	0.0	⋯	⋯
57779.0066	2.10	0.0	⋯	⋯
57784.9812	2.04	0.0	⋯	⋯
57787.9734	1.69	0.0	⋯	⋯
57791.9718	1.73	0.0	⋯	⋯
57794.9856	1.87	0.0	⋯	⋯
57796.0239	1.73	0.0	⋯	⋯
57800.9306	1.82	0.0	⋯	⋯
57806.9195	−5.22	0.5	9.58	0.5
57807.0310	−5.49	0.5	9.78	0.5
57807.9270	−8.13	1.0	12.20	1.0
57808.9264	−13.32	1.0	17.70	1.0
57809.0310	−14.38	1.0	18.45	1.0
57809.9104	−24.74	1.0	28.24	1.0
57809.9410	−25.10	1.0	28.89	1.0
57809.9810	−25.59	1.0	29.64	1.0
57810.0010	−25.92	1.0	30.04	1.0
57810.0261	−26.23	1.0	30.62	1.0
57812.0272	−36.62	1.0	40.93	1.0
57813.9412	−18.22	1.0	21.99	1.0
57813.9486	−18.14	1.0	21.91	1.0
57813.9612	−18.16	1.0	21.61	1.0

Table 2
(Continued)

HJD—2400000	K_1(km s^{-1})	K_1 Weight	K_2(km s^{-1})	K_2 Weight
57813.9812	−17.91	1.0	21.82	1.0
57814.0012	−17.87	1.0	21.64	1.0
57814.0262	−17.65	1.0	21.46	1.0
57814.8998	−14.53	1.0	18.01	1.0
57814.9612	−14.29	1.0	17.77	1.0
57816.8990	−9.81	1.0	13.04	1.0
57816.9613	−9.54	1.0	12.88	1.0
57818.9437	−7.16	1.0	10.55	1.0
57819.0214	−6.92	1.0	10.58	1.0
57819.8909	−6.16	1.0	10.00	1.0
57820.0164	−6.29	1.0	9.65	1.0
57820.9126	−5.58	1.0	9.25	1.0
57820.9614	−5.66	1.0	9.02	1.0
57821.9110	−5.13	1.0	8.60	1.0
57822.0164	−5.20	1.0	8.45	1.0
57822.8834	−4.41	0.5	8.30	0.5
57823.0165	−4.41	0.5	8.24	0.5
57823.8719	−4.43	0.5	7.54	0.5
57824.8732	−3.92	0.5	7.29	0.5
57825.8731	−3.78	0.0	6.69	0.0
57826.8731	−3.57	0.0	6.28	0.0
57827.8731	−3.22	0.0	6.40	0.0
57829.8737	−2.25	0.0	6.16	0.0
57830.8733	−2.21	0.0	5.72	0.0
57831.8751	−2.01	0.0	5.94	0.0
57832.8779	−1.90	0.0	5.64	0.0
57843.0072	2.00	0.0	…	…
57863.8002	1.96	0.0	…	…
58139.0144	−6.39	1.0	10.50	1.0
58139.0305	−6.75	1.0	10.50	1.0
58140.0218	−9.83	1.0	14.53	1.0
58141.0305	−17.9	1.0	22.14	1.0
58141.0379	−17.87	1.0	22.26	1.0
58142.0185	−34.15	1.0	38.59	1.0
58142.0257	−34.08	1.0	38.88	1.0
58142.0329	−34.38	1.0	38.88	1.0
58142.0403	−34.53	1.0	39.20	1.0
58142.0474	−34.79	1.0	39.25	1.0
58142.9958	−46.30	1.0	50.47	1.0
58143.0031	−46.20	1.0	50.50	1.0
58143.0185	−46.10	1.0	50.44	1.0
58143.0257	−46.17	1.0	50.28	1.0
58143.0329	−46.11	1.0	50.16	1.0
58144.0185	−30.77	1.0	35.07	1.0
58144.0257	−30.99	1.0	34.96	1.0
58144.0329	−30.74	1.0	34.90	1.0
58144.0402	−30.42	1.0	34.90	1.0
58144.0474	−30.44	1.0	34.71	1.0
58144.9979	−21.14	1.0	25.36	1.0
58145.0051	−21.38	1.0	25.10	1.0
58145.0185	−21.50	1.0	24.95	1.0
58145.0257	−21.22	1.0	25.10	1.0
58145.0329	−21.21	1.0	24.88	1.0
58146.0306	−15.98	1.0	20.09	1.0
58146.0415	−16.00	1.0	19.78	1.0
58147.0101	−12.42	1.0	16.76	1.0
58147.0415	−12.34	1.0	16.56	1.0
58148.0415	−10.33	1.0	14.17	1.0
58149.0041	−8.88	1.0	12.37	1.0
58149.0415	−8.61	1.0	12.47	1.0
58150.0119	−7.23	1.0	11.36	1.0
58150.0416	−7.19	1.0	11.48	1.0
58150.9796	−6.43	1.0	10.86	1.0
58151.0416	−6.18	1.0	10.42	1.0

Table 2
(Continued)

HJD—2400000	K_1(km s^{-1})	K_1 Weight	K_2(km s^{-1})	K_2 Weight
58152.0160	−5.69	1.0	9.72	1.0
58152.0416	−5.92	1.0	9.49	1.0
58153.9725	−4.66	0.5	8.34	0.5
58154.0416	−4.67	0.5	8.50	0.5
58154.9681	−4.19	0.5	8.09	0.5
58155.0416	−4.21	0.5	7.95	0.5

Note. Spectroscopic observations for HR 7345 obtained from 2014 to 2018 with the 2 m AST and a fiber-fed echelle spectrograph at Fairborn Observatory. The velocity from the single, partially resolved ELODIE spectrum acquired in 2000 November (Prugniel et al. 2007) is also listed.

(This table is available in machine-readable form.)
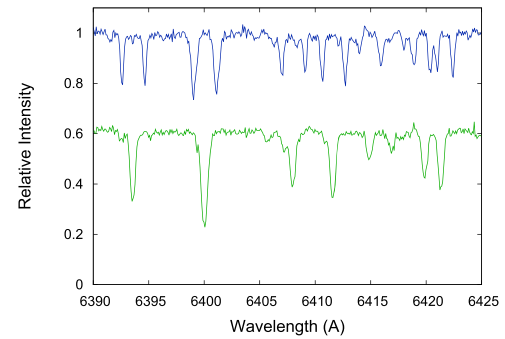
Figure 1. A portion of an echelle order for HJD 2458142 (upper, double-lined spectrum) and HJD 2458153 (lower, single-lined spectrum). The upper spectrum is our observation closest to maximum velocity separation. The lower spectrum, shifted downward for clarity, has an orbital phase of about 0.03 and has a velocity separation of 13 km s^{-1}. The latter spectrum is representative of spectra with very blended lines from which we obtained useful velocity measurements. Spectra with the components having smaller velocity separations had systematic residuals and were not used in our orbital solutions.

period of about 330 days rather than a much more circular orbit with twice that period.

With the results of a preliminary joint astrometric–spectroscopic orbital solution, preparations were made to attempt spectroscopic observations during the next periastron passage that was to occur in the latter half of 2017 February. However, given the near 11-month period, that predicted periastron passage would occur less than 50 days after HR 7345 reached the same R.A. as the Sun. In most cases observations so close to the Sun are precluded. However, when the Sun and HR 7345 have the same R.A., they have a decl. difference of 59°. This large difference enabled us to acquire spectra of HR 7345 during the periastron passages of 2017 February and 2018 January.

Despite the short observing window at the very end of the nights in 2017 February, we attempted to get multiple observations of HR 7345 each night for the two-week period around predicted periastron. Although the night of maximum velocity separation was cloudy, we were able to obtain spectra on the adjacent nights. However, having missed the night of maximum velocity separation in 2017 February, we decided to obtain spectra of the system at its next periastron passage in 2018 January when it was even closer to the Sun. Fortunately, the weather cooperated, and we successfully acquired multiple spectra of HR 7345 on nearly every night when the double

Table 3
Orbital Parameters for HR 7345

Parameter	SB2 Orbit	VB Orbit	Joint Fit
P (days)	331.607 ± 0.0037	331.601 ± 0.075	331.609 ± 0.0037
T (HJD)	58142.692 ± 0.0029	58142.681 ± 0.012	58142.690 ± 0.0027
e	0.93209 ± 0.00013	0.9324 ± 0.0011	0.9322 ± 0.00013
a (mas)	...	47.58 ± 0.11	47.432 ± 0.035
i (°)	...	29.6 ± 1.2	29.48 ± 0.86
Ω (°)	...	176.2 ± 6.4	181.046 ± 0.092
ω_A (°)	169.934 ± 0.077	175.4 ± 7.3	169.888 ± 0.075
K_A (km s^{-1})	25.535 ± 0.047	...	25.555 ± 0.047
K_B (km s^{-1})	25.927 ± 0.047	...	25.947 ± 0.048
γ (km s^{-1})	1.827 ± 0.030	...	1.827 ± 0.031

Note. The angle between the ascending node and periastron, as referenced to HR 7345 B (the typical reference for visual orbits), is given by $\omega_B = \omega_A + 180° = 349°.89 \pm 0°.08$.

lines were resolved including the night of maximum velocity separation. Thus, the spectroscopic solution is well constrained.

We first determined spectroscopic orbits of the individual components with SB1, a program that iterates the orbital elements by differential corrections (Barker et al. 1967). To obtain a simultaneous two-component solution, we used SB2, which is a slightly modified version of SB1.

Because of its very high eccentricity, the orbital fit is dominated by the velocities near periastron that are determined from component lines that are at least partly resolved at our resolution. This is a window of about 15 days and so covers only about 5% of the orbit. We tried various solutions with different weights for those velocities that were determined for the completely blended double lines. In the final spectroscopic solution, we assigned zero weight to the velocities of those observations that were measured as single-lined. However, for the spectra having broadened but completely blended lines, the velocity weighting was more problematic. Velocities for many of the spectra with very blended lines that were measured as double lined show systematic velocity residuals (Figure 3) and so were not used in the final solution. In the final orbit, all velocity measurements, whether single or double, between phases 0.042 and 0.985 were given zero weight. Radial velocities from the 12 most blended remaining observations (see Figure 1) were given weights of 0.5, while all other velocities were given unit weights. The solution given by only the spectroscopic data is listed in column two in Table 3.

3.3. Combined Solution

We also fit an orbit simultaneously to the visual and spectroscopic data. In the joint fit, we applied the measurement weights determined based on the individual orbit fits. To give equal weight to each set of data, we scaled the uncertainties from each set to force the reduced χ_ν^2 to equal unity. We then computed the simultaneous orbital fit following a similar Newton-Raphson technique as described in Section 3.1, but expanded to fit all 10 orbital parameters. The parameters from the joint fit are listed in the last column of Table 3. The uncertainties were computed from the diagonal elements of the covariance matrix. Figures 2 and 3 show the measurements compared with the joint orbital fit.

4. Orbital Parameters

The parameters from the joint orbital fit are mostly consistent within their uncertainties with those determined from the individual fits to the visual and spectroscopic data. The values for P, T, e, and ω_A are constrained more strongly by the radial velocity measurements. The changes in i, Ω, and ω_A in the visual only fit compared with the joint fit are a result of the tighter constraints on e and ω_A provided by the radial velocities. Table 4 gives the masses and distance computed from the orbital parameters. Our combined orbital solution after the 2017 February periastron passage produced an inclination of $32°.4 \pm 1°.3$ and individual stellar masses of 0.73 and 0.72 $M_\odot$. Such values are significantly lower than the value of $\sim$0.95 $M_\odot$ expected for a spectral type of G5 V (Gray et al. 2003). However, the dynamical masses are highly sensitive to the low inclination. After obtaining interferometric observations as the system passed through the 2018 periastron, the revised orbit produces masses of 0.941 ± 0.076 and $0.926 \pm 0.075 M_\odot$, which are very close to the value expected for a G5 V star. The orbital parallax of 41.1 ± 0.8 mas is larger than the Hipparcos parallax of 39.39 ± 0.33 mas, which has no flag for binarity listed in any of the revisions of the data set (van Leeuwen 2008). Similarly, the Gaia DR2 (Gaia Collaboration et al. 2016) parallax (39.646 ± 0.098 mas) is closer to the Hipparcos values rather than the orbital parallax. While there is not a direct flag in the Gaia DR2 (Luri et al. 2018), the data collected does show abnormally high astrometric χ^2, "goodness of fit", and excess noise values indicate a statistically poor fit, likely due to the not-quite equal magnitude of the system's components.

5. High-eccentricity Binaries Comparisons

Comparing the orbital elements for HR 7345 to systems listed in the Ninth Catalog of Spectroscopic Binary Orbits (Pourbaix et al. 2004) and the Sixth Catalog of Orbits of Visual Binary Stars (Hartkopf et al. 2001), one immediately sees that HR 7345 stands out. Sorting by eccentricity, it ranks as the 12th most eccentric in the spectroscopic catalog, and is 83rd in the visual binary catalog, but of those systems that are more eccentric, none has such a short period. The closest comparable systems in the visual catalog have periods on the order of 800 days (HD 66751 and HD 212029). In the spectroscopic catalog, the shortest-period system with a larger eccentricity than HR 7345 is HD 137763, which has a period of 890 days, while with a period of 298 days, HD 89707 is a system with a similar period and very high but smaller eccentricity than HR 7345. Both of the visual systems have astrometric solutions from Hipparcos data, but the binaries were published with two
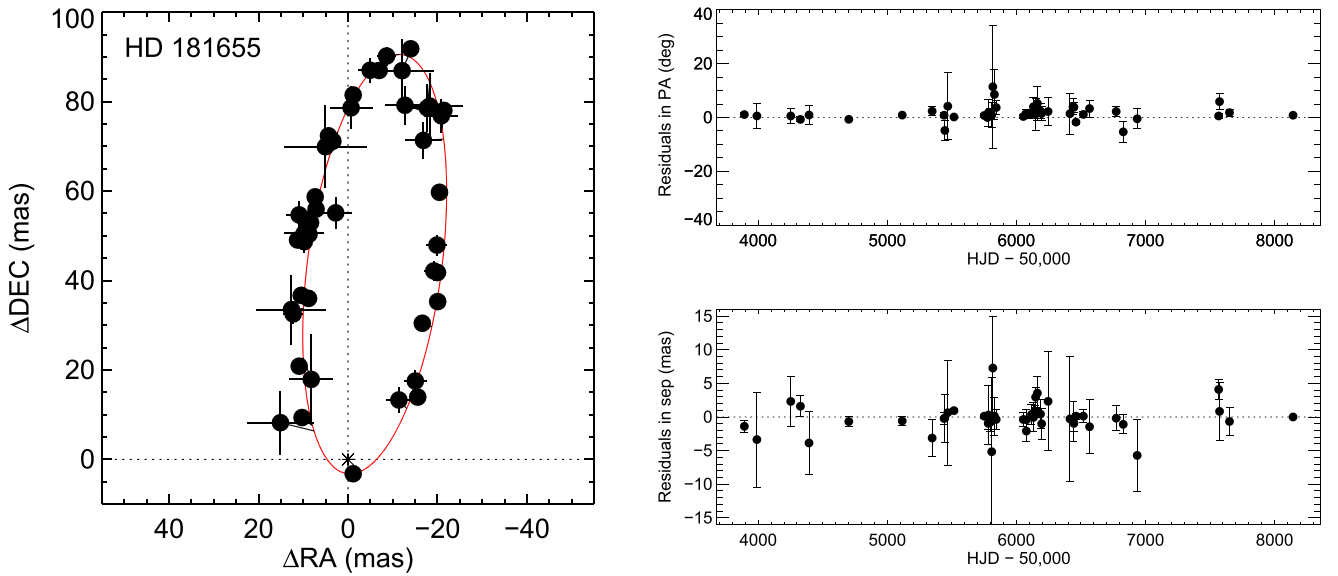
Figure 2. Left panel: orbital motion of HR 7345 A relative to B as measured with CHARA Classic and CLIMB. Overplotted in red is the best-fit orbit computed from a simultaneous fit to the CHARA measurements and the spectroscopic radial velocities. Right panel: residuals between the measured position angle and separation compared with the best-fitting orbit.
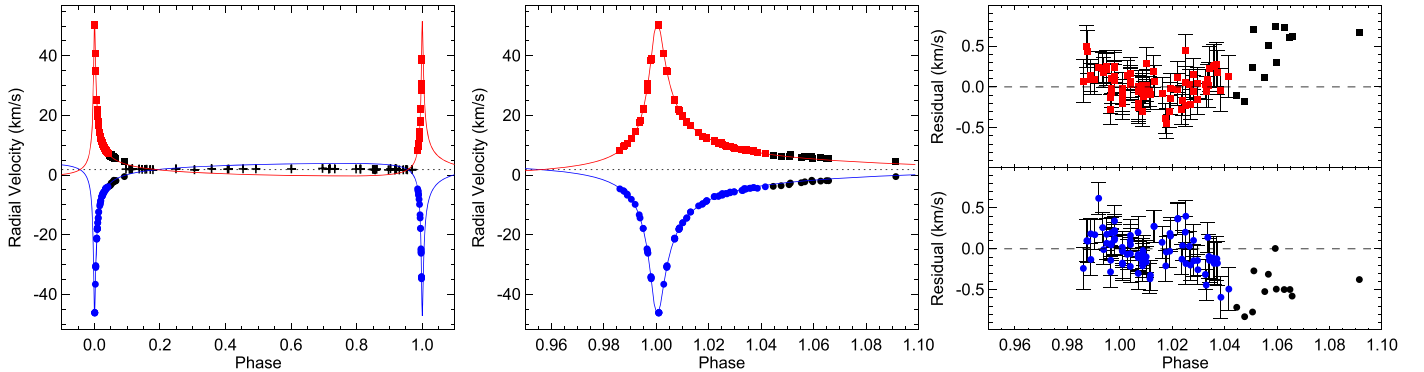

Figure 3. Radial velocity measurements for HR 7345 A (blue circles) and B (red squares). The solid line is the best-fitting orbit computed from a simultaneous fit to the CHARA measurements and the spectroscopic radial velocities. The center-of-mass velocity is shown as a dotted line. The filled black symbols are the individual velocities for the two components that were given zero weight because the lines of the two components were severely blended. The black crosses show the single-lined velocity measurements. The middle panel shows a zoomed in view of the phase-wrapped radial velocity peak. The panels on the right show the residuals between the measured radial velocities and the orbital fit for each component.

Table 4
Stellar Properties for HR 7345

Parameter	Value
M_A ($M_\odot$)	0.941 ± 0.076
M_B ($M_\odot$)	0.926 ± 0.075
d (pc)	24.34 ± 0.45
π (mas)	41.08 ± 0.77

differing orbits for each system with discrepancies between the eccentricities ($e = 0.97^{+0.02}_{-0.56}$ and $e = 0.56^{+0.43}_{-0.27}$ for HD 66751, $e = 0.92^{+0.07}_{-0.34}$ and $e = 0.99^{+0.00}_{-0.19}$ for HD 212029) in two different tables in the same paper (Goldin & Makarov 2006). For the spectroscopic systems, HD 89707 is only single-lined and its companion is a brown dwarf candidate. The initial orbit from Duquennoy & Mayor (1991) has an eccentricity of 0.927 ± 0.014 but a more recent orbit by Sahlmann et al. (2011) reduced it to $0.900^{+0.039}_{-0.035}$. However, even this more recent orbit remains questionable as the rapid nodal passage is

very poorly covered. Likely the best system for comparison is HD 137763, which has both a visual and spectroscopic solution with a very similar "extreme orbit" paper espousing the superlative eccentricity of 0.976 (Strassmeier et al. 2013) from high precision spectroscopy followed by a visual and combined solution from Tokovinin (2016). While the eccentricity of HD 137763 is more extreme, the period of HR 7345 is significantly shorter while still very eccentric.

Griffin (2003) reviewed the limited number of spectroscopic binaries with published eccentricities greater than 0.9 that were known at that time. He then extensively discussed the great difficulty of identifying such systems spectroscopically pointing out that the discoveries are influenced by observational selection effects and the pure luck of observing a system in such a small phase window of the orbit. As discussed in Section 1, of the dozens of spectroscopic observations acquired before our spectroscopic observations began, only one was at a phase that showed partially resolved components. Thus, in the case of our efforts on HR 7345, its binary nature was first detected interferometrically rather than spectroscopically.

Griffin (2003) goes on to mention that there is a second selection effect, as the longitude of periastron of previously identified high-eccentricity binaries is clustered around 90° and 270°, because the slow velocity change resulting from those longitudes of periastron provides a much wider observational window to catch a double-lined phase than the perpendicular case. The lone ELODIE observation of HR 7345 with its partially resolved components (Prugniel et al. 2007) produced no follow-up campaign to establish its orbit. Thus, it is indeed fortunate that the system was independently discovered to be a binary by visual means. Even knowing that HR 7345 is a binary, it was quite difficult over the course of 12 years to determine the correct visual orbit for a nearly equal component binary having almost a one-year period. Indeed, the determination of an accurate periastron only occurred after a decade of periodic observation and with the most recent periastron occurrence barely observable before the system goes into hiding behind the Sun for the next three years.

Given the extreme eccentricity of HR 7345, the original architecture of this binary system was almost certainly very different than it is now. There are several mechanisms that could produce such large eccentricities in a nearly equal mass binary, all of which involve a third or fourth component. Without the ability to probe the initial conditions, it is hard to say how many components the system originally had during formation. However, the most probable explanation for just the eccentricity extreme is likely the Kozai–Lidov mechanism (see Kozai 1962; Lidov 1962), where the system was previously a non-coplanar triple with a less massive wide component, likely smaller than the two other components with sufficient inclination to the inner orbit to cause oscillations in the eccentricity increasing to current levels and then being ejected from the system by a close encounter (Anosova 1986). During a recent check of proper motions and distance of the surrounding area after the Gaia DR2 was published earlier this year (HR 7345: $\mu_\alpha = -61.524 \pm 0.191$ mas yr^{-1}, $\mu_\delta = -183.668 \pm 0.211$ mas yr^{-1}), an amended entry was placed at the top of the list. Conveniently, this is a candidate (2MASS J19193649+3720077) for this interaction at only 35 arcsec in angular distance. Previously listed as only an X-ray and IR source, the Gaia DR2 added distance, proper motion, and magnitude ($\pi = 38.88 \pm 0.23$ mas, $\mu_\alpha = -53.47 \pm 0.51$ mas yr^{-1}, $\mu_\delta = -204.55 \pm 0.49$ mas yr^{-1}, and V-mag = 11.484 K-mag = 7.87) very similar to that of HR 7345. Due to it being an X-ray emitter, moderately bright in the IR, and faint in the visible, the object is likely to be a chromospherically active M-dwarf, which fits the speculated criteria for the instigator of the Kozai–Lidov mechanism. An ejection of this type would certainly explain the rare high eccentricity. Further investigation of the components and the formation mechanisms could be followed up in further studies.

6. Conclusion and Discussion

Prior to the observations taken in 2018 January, the calculated orbit left many open issues because of the unobserved part of the orbit around periastron. The value and large error in inclination due to the missing part of the orbit produced masses that were significantly lower than expected, but a large enough error bar to include the canonical masses for stars of that spectral classification. While the data and orbit were deemed solid enough to publish as they were, we decided to make one more attempt if the weather permitted to improve the combined orbit. The weather over Fairborn Observatory proved to be significantly more cooperative in obtaining spectra of the system during the 2018 periastron and filled in the missing single day of phase coverage. Observations with the CHARA Array were setup for the four days on either side of the predicted periastron passage, but due to wind, clouds, and humidity, we were only able to obtain a single data set directly on periastron. Fortunately, the results from this single night proved to be very valuable and allowed a final recalculation of the orbit, which provided significant reductions in the inclination value and associated errors. While the 2018 observations significantly improved the orbit and resulting masses, those masses, although consistent with the spectral type, have relatively large uncertainties.

With the use of our orbital period and component masses, we obtained from Kepler's third law a semimajor axis of 1.156 au. The system's large eccentricity produces a periastron separation of 0.079 au or 16.9 $R_\odot$. Hut (1981) has shown that for stars in an eccentric orbit the rotational angular velocity of an individual star will tend to synchronize with that of the orbital motion at periastron. He called this situation pseudosynchronous rotation. To see whether the components of HR 7345 have achieved that state, we first determined the projected rotational velocities of the components from our rotational broadening fits and found $v \sin i$ values of 2.6 ± 1.0 km s^{-1} for each component. If the rotational and orbital axes are parallel, as is generally assumed for stars in binary systems, then our orbital inclination of 29°.5 produces rotational velocities of 5.3 ± 1.0 km s^{-1}. From Kepler's third law, the pseudosynchronous period is 5.88 days. If we adopt radii of 0.95 $R_\odot$ for the G5 dwarfs, then the predicted pseudosynchronous velocities of the components are 8.2 km s^{-1}. Thus, although the rotational velocities that we have determined for the two components of HR 7345 are larger than typical values of about 2–3 km s^{-1} for most late-type stars (Valenti & Fischer 2005), the components of HR 7345 have not yet reached pseudosynchronous rotation.

In a review of precise masses and radii for normal stars, Torres et al. (2010) cataloged 23 systems with both visual and spectroscopic orbits that produced component stellar masses determined to better than 3%. As listed in Table 4, the masses of HR 7345 have a 9% uncertainty. As most of the error in the masses is tied to the inclination, additional observations around periastron should refine the orbit further and decrease the mass uncertainty. With the current orbital elements, the ideal time to observe the system is the during the week before and after periastron, when the system is separated by less than 15 mas. Such observations will be attempted around 2021 September 11, during the next easily observable periastron passage.

ORCID iDs

C. D. Farrington ⓘ https://orcid.org/0000-0001-9939-2830
Francis C. Fekel ⓘ https://orcid.org/0000-0002-9413-3896
G. H. Schaefer ⓘ https://orcid.org/0000-0001-5415-9189
T. A. ten Brummelaar ⓘ https://orcid.org/0000-0002-0114-7915

References

Ambartsumian, V. A. 1937, AZh, 14, 207
Anosova, J. P. 1986, Ap&SS, 124, 217
Barker, E. S., Evans, D. S., & Laing, J. D. 1967, RGOB, 130, 355
Barnes, T. G., III, Moffett, T. J., & Slovak, M. H. 1986, PASP, 98, 223
Bate, M. R. 2009, MNRAS, 392, 590
Beavers, W. I., Eitter, J. J., Ketelsen, D. A., & Oesper, D. A. 1979, PASP, 91, 698
Bourges, L., Lafrasse, S., Mella, G., et al. 2014, in ASP Conf. Ser. 485, Astronomical Data Analysis Software and Systems XXIII, ed. N. Manset & P. Forshay (San Francisco, CA: ASP), 223
Crifo, F., Jasniewicz, G., Soubiran, C., et al. 2010, A&A, 524, A10
Crissman, B. G. 1957, AJ, 62, 280
Duflot, M., Figon, P., & Meyssonnier, N. 1995, A&AS, 114, 269
Duquennoy, A., & Mayor, M. 1991, A&A, 248, 485
Duquennoy, A., Mayor, M., & Halbwachs, J. L. 1991, A&AS, 88, 281
Eaton, J. A., & Williamson, M. H. 2007, PASP, 119, 886
Farrington, C. D., ten Brummelaar, T. A., Mason, B. D., et al. 2010, AJ, 139, 2308
Farrington, C. D., ten Brummelaar, T. A., Mason, B. D., et al. 2014, AJ, 148, 48
Fehrenbach, C., Duflot, M., Mannone, C., Burnage, R., & Genty, V. 1997, A&AS, 124, 255
Fekel, F. C., & Griffin, R. F. 2011, Obs, 131, 283
Fekel, F. C., Tomkin, J., & Williamson, M. H. 2009, AJ, 137, 3900
Finsen, W. S. 1936, MNRAS, 96, 862
Gaia Collaboration, Brown, A. G. A., Vallenari, A., et al. 2016, A&A, 595, A2
Goldin, A., & Makarov, V. V. 2006, ApJS, 166, 341
Gray, R. O., Corbally, C. J., Garrison, R. F., McFadden, M. T., & Robinson, P. E. 2003, AJ, 126, 2048
Griffin, R. F. 2003, Obs, 123, 344
Griffin, R. F. 2012, JApA, 33, 29
Halbwachs, J. L., Mayor, M., Udry, S., & Arenou, F. 2003, A&A, 397, 159
Halliday, I. 1955, ApJ, 122, 222
Hartkopf, W. I., Mason, B. D., & Worley, C. E. 2001, AJ, 122, 3472
Holmberg, J., Nordström, B., & Andersen, J. 2009, A&A, 501, 941
Hut, P. 1981, A&A, 99, 126
Kluska, J., Kraus, S., Davies, C. L., et al. 2018, AJ, 855, 44
Kozai, Y. 1962, AJ, 67, 591
Lacy, C. H. S., & Fekel, F. C. 2011, AJ, 142, 185
Lidov, M. L. 1962, P&SS, 9, 719
Luri, X., Brown, A. G. A., Sarro, L. M., et al. 2018, arXiv:1804.09376
Mason, B. D., Wycoff, G. L., Hartkopf, W. I., Douglass, G. G., & Worley, C. E. 2001, AJ, 122, 3466
McAlister, H. A., Hartkopf, W. I., Hutter, D. J., & Franz, O. G. 1987, AJ, 91, 688
Monnier, J. D., Zhao, M., Pedretti, E., et al. 2011, ApJ, 742, L1
Nidever, D. L., Marcy, G. W., Butler, R. P., Fischer, D. A., & Vogt, S. S. 2002, ApJS, 141, 503
Nordström, B., Mayor, M., Andersen, J., et al. 2004, A&A, 418, 989
Perryman, M. A. C., Lindegren, L., Kovalevsky, J., et al. 1997, A&A, 323, L49
Pourbaix, D., Tokovinin, A. A., Batten, A. H., et al. 2004, A&A, 424, 727
Prugniel, P., Soubiran, C., Koleva, M., & Le Borgne, D. 2007, yCat, 3251, 0
Raghavan, D., McAlister, H. A., Henry, T. J., et al. 2010, ApJS, 190, 1
Sahlmann, J., Ségransan, D., Queloz, D., et al. 2011, A&A, 525, A95
Scarfe, C. D. 2010, Obs, 130, 214
Schaefer, G. H., Hummel, C. A., Gies, D. R., et al. 2016, AJ, 152, 213
Schaefer, G. H., Simon, M., Beck, T. L., Nelan, E., & Prato, L. 2006, AJ, 132, 2618
Soubiran, C., Jasniewicz, G., Chemin, L., et al. 2013, A&A, 552, A64
Strassmeier, K. G., Weber, M., & Granzer, T. 2013, A&A, 559, A17
ten Brummelaar, T. A., McAlister, H. A., Ridgway, S. T., et al. 2005, ApJ, 628, 453
ten Brummelaar, T. A., Sturmann, J., Ridgway, S. T., et al. 2013, JAI, 2, 1340004
Tokovinin, A. 2016, AJ, 152, 138
Tokovinin, A., & Kiyaeva, O. 2016, MNRAS, 456, 2070
Torres, G., Andersen, J., & Giménez, A. 2010, A&ARv, 18, 67
Valenti, J. A., & Fischer, D. A. 2005, ApJS, 159, 141
van Belle, G. T., van Belle, G., Creech-Eakman, M. J., et al. 2008, ApJS, 176, 276
van Leeuwen, F. 2008, A&A, 474, 653
Young, R. K. 1945, PDDO, 1, 311